RSC Advances

PAPER

View Article Online
View Journal | View Issue

Cite this: *RSC Adv.*, 2021, **11**, 22034

Dual-ion substituted $(MeY)_3(AlSi)_5O_{12}$:Eu garnet phosphors: combinatorial screening, reductive annealing, and luminescence property

Zhehan Zheng,[ab] Mingxue Deng,[ac] Caiyan Wang,[ac] Xiang Zhang,[ac] Qian Liu,*[ac] Xiaoke Xu[a] and Le Gao[a]

In recent years, the efficiency of combinatorial methods has been utilized to accelerate the finding or screening of inorganic materials. In this work, based on the double substitution strategy of the cation ions Me^{2+}/Si^{4+}, a series of $Me_yY_{3-y}Al_{5-y}Si_yO_{12}:Eu_x$ garnet phosphors (MeYASG:Eu, Me = Mg, Ca, Sr, Ba) were rapidly prepared and screened by a combinatorial method in microreactor arrays. Through parallel experiments of solid-state synthesis, the reliability of the combinatorial screening was verified and an optimal composition of $CaY_2Al_4SiO_{12}:Eu_{0.03}$ (CYASG:Eu) with advanced luminous intensity was obtained. Annealing experiments under air and reductive atmospheres were performed and demonstrated the controllability and reversibility of the $Eu^{3+} \leftrightarrow Eu^{2+}$ valence transition process, thus realizing the tuning of the dominant emission from divalent Eu^{2+} or trivalent Eu^{3+}. The optimal CYASG:Eu sample showed excellent thermal quenching resistance after annealing at 800 °C for 1 h in a reducing atmosphere. The abnormal intensity of PL increased by 10% in the 50–100 °C region, and retained 63% of the initial value at 250 °C. With the assistance of thermoluminescence characterization, the complementary effect of the release of captured electrons or charge carriers in trap levels on the abnormal increase of PL intensity during the high-temperature luminescence process was revealed. By combination of the double substitution strategy of cations and annealing, a new approach is proposed to creating the coexistence of activator Eu ions with a mixed-valence state. Also, the prepared CYASG:Eu phosphors have promising applications in fields such as plant light supplements in greenhouses and plant factories and as luminescent materials for energy-saving light sources.

Received 7th April 2021
Accepted 7th June 2021

DOI: 10.1039/d1ra02705k

rsc.li/rsc-advances

1. Introduction

Yttrium aluminum garnet (YAG, $Y_3Al_5O_{12}$)-based phosphors are among the most common fluorescent materials. With a cubic phase structure, YAG-based phosphors have demonstrated isotropic thermal expansion, stable optical properties, and no birefringence effect.[1–5] Rare-earth ions, as activators or substitution elements in the main lattice of YAG, can enrich the luminescent composition by colorful emissions from 5d–4f and 4f–4f transitions under blue or ultraviolet light excitation.[6–8] Therefore, rare-earth-ion-doped YAG phosphors, such as cerium-doped yttrium aluminum garnet (YAG:Ce) phosphors, are widely applied in white-light-emitting diodes (WLEDs) by encapsulating them on blue-emitting LED chips. Due to its irreplaceable performance in various optics applications, in recent years, many researchers have focused on enriching the emission properties of YAG systems.

Taking YAG:Ce as an example, it could be summarized as enriching the emission of YAG-based phosphors in two ways. One is to change the crystal field strength of the host lattice by cation substitution;[9–12] for instance, Y^{3+} or Al^{3+} sites replaced by other cations will change the crystal field environment around activator ions and then result in a red or blue shift of its emission peak. For example, occupying Y^{3+} (1.159 Å, ligand number VIII) sites with the larger radius ion Gd^{3+} (1.193 Å, ligand number VIII) can tune the emission peak of Ce^{3+} from the normal 530 nm to 565 nm.[13,14] Also, the dual-ion Mg^{2+} (0.86 Å, ligand number VI)/Si^{4+} (0.4 Å, ligand number IV) replacement for Al^{3+} (0.675 Å, ligand number VI)/Al^{3+} (0.53 Å, ligand number IV) cation pair can make the emission peak shift from 530 nm to 615 nm.[15] However, as the Ce^{3+} emission peak is shifted, these cation-substitution strategies inevitably encounter the situation of reduced emission intensity. Another strategy is the co-doping of activator ions such as Cr^{3+}, Pr^{3+}, and Sm^{3+}.[2,3,16] In general, co-doped activator ions tend to have weak absorption in the blue-light region. Nevertheless, the energy transfer between activator

[a]*The State Key Laboratory of High Performance Ceramics and Superfine Microstructure, Shanghai Institute of Ceramics, Chinese Academy of Sciences, Shanghai 200050, China. E-mail: qianliu@mail.sic.ac.cn*

[b]*College of Materials Science and Engineering, Fuzhou University, Fuzhou, Fujian 350116, China*

[c]*Center of Materials Science and Optoelectronics Engineering, University of Chinese Academy of Science, Beijing 100049, China*

ions will also cause an emission decrease owing to the transfer efficiency between different donor–receiver pairs.

As another activator ion that has been studied in the YAG system, the Eu ion has a broad emission ranging from blue to red in various substrates.[17] Additionally, Eu ions can be efficiently excited by deep ultraviolet (especially 254 nm), near ultraviolet (365 nm, 380 nm), and even visible light. The promising photoluminescence spectrum (PL) and excitation spectrum (PLE) distribution greatly expand its potential applications.[18–21] Further, it has become a new research direction to obtain emissions from mixed-valence Eu ions in a single substrate. So far, many efforts have been made to realize the doping of divalent Eu ions in the YAG system, such as by means of charge compensation, crystal engineering and other specific approaches.[22–27] However up to now, the coexistence of mixed-valence Eu ions has rarely been reported in the YAG system, and most of the existing research can only induce Eu^{2+}-ion doping through routes involving a high heating temperature or long sintering time with a reducing agent or reducing atmosphere assistance. It was not until 2017 that Pan *et al.* first reported a series of YAG-based hosts suitable for divalent activator ions stabilization in a YAG system by combining a double substitution and charge-compensation strategy that was achieved with Ce^{3+} and Mn^{2+} co-doping.[28]

We combined the helpful concepts above and tried to further find a substituted YAG garnet matrix suitable for the coexistence of Eu ions with mixed valence. This idea brought difficulties in designing the composition and in the screening due to the introduction of substitution ions and valence transitions within the YAG system. Hence, a combinatorial approach was employed for the rapid preparation and screening of material libraries with various YAG-based compositions.

Considering that the formula of YAG-based phosphors can be simplified as $A_3B_2C_3O_{12}$, where A, B, and C represent dodecahedral, octahedral, and tetrahedral-coordinated sites, respectively, in our research, a series of alkaline earth metal ions (Me) were designed to enter the A sites to replace the Y^{3+}, providing sites that could be occupied by the reduced Eu^{2+} ions. Also, Si^{4+} ions were designed to enter the C sites to replace Al^{3+} as charge compensators for substituting divalent ions (Me) and reduced Eu^{2+} ions after annealing. Further, phosphor libraries with the formula of $Me_yY_{3-y}Al_{5-y}Si_yO_{12}:Eu_x$ (MeYASG:Eu, Me = Mg, Ca, Sr, Ba; $x = 0.001$–0.05; $y = 0, 0.5, 1$) were synthesized by a combinatorial method in parallel microreactors and then fluorescent screening was carried out to search for the optimal compositions showing strong emission. Large-scale powder samples with the screened optimal compositions $CaY_2Al_4SiO_{12}:Eu_{0.03}$ were prepared by multi-step solid-state reactions in air and also with the assistance of a weak reducing atmosphere to realize Eu doping with mixed valence. The spectral characterization results further verified the reliability of the combinatorial screening of the optimal compositions. The stability, controllability, and reversibility of Eu^{2+} formation in the host were investigated by annealing under different conditions. Additionally, the luminescence properties, spectral tuning, and thermoluminescence of the optimized compositions were systematically investigated.

2. Experiment

2.1 Combinatorial preparation and screening of the MeYASG:Eu material libraries

First, a dual-ion substituted MeYASG:Eu (Me = Mg, Ca, Sr, Ba) phosphor library, a {9 × 12} array, was designed and prepared, whose chemical composition could be described as $Eu_x:Me_yY_{3-y}Al_{5-y}Si_yO_{12}$ ($x = 0.001$–0.05 and $y = 0, 0.5, 1$). Based on the designed composition map, the library was rapidly dripped through a home-designed combinatorial synthesizer, with a schematic diagram of the combinatorial synthesizer shown in Fig. 1. The motor-controlled injection system could transfer the calculated amount of different liquid precursors onto the arrayed microreactors in the sintered alumina substrate. The capacity of each microreactor was 550 μL, and the tolerance of the injection module could be controlled in the range of 1–15 μL.

The needed precursor solutions of Eu ions or Y ions were prepared by dissolving the oxide Eu_2O_3 or Y_2O_3 in nitric acid, while the precursor solutions of Mg, Ca, Sr, Ba alkaline earth metal ions, and Al ions were prepared by dissolving their corresponding nitrates ($Mg(NO_3)_2\cdot 6H_2O$, $Ca(NO_3)_2\cdot 4H_2O$, $Sr(NO_3)_2$, $Ba(NO_3)_2$, and $Al(NO_3)_3\cdot 9H_2O$) in deionized water, and the Si^{4+}-ion precursor solution was prepared by dissolving TEOS ($C_8H_{20}O_4Si$) in the mixture of alcohol and deionized water. After the on-demand injection of all the designed compositions, the liquid mixtures in microreactors were agitated in an *in situ* ultrasonic bath for 30 min and then *in situ* heated up to 80 °C for 3 h to vaporize water and alcohol. Finally, the mixed solution in each microreactor was dried to a gel state. The prepared library was further calcined at 600 °C for 2 h in an air atmosphere to realize nitrate pyrolysis. After the first calcination, the powder precursors within the microreactors were thoroughly ground and further calcined at 1300 °C for 2 h in an air atmosphere to obtain the expected library of MeYASG:Eu phosphors with a series of composition variations.

The prepared library was entirely irradiated by a Hg lamp with a 254 nm broadband filter and the corresponding emitting image was recorded using a digital camera (Canon EOS 600D) to evaluate the emission intensity for all the samples in the library. Based on the captured luminous image, optimal compositions showing higher emission intensities were selected as the "clue

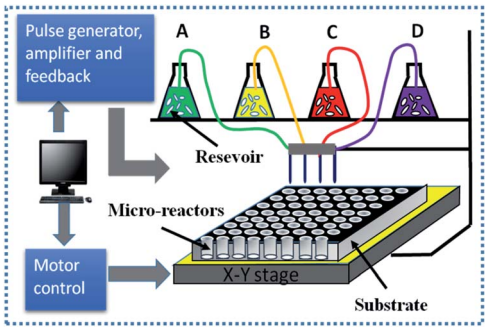

Fig. 1 Schematic diagram of the combinatorial synthesizer used with the materials library.

values" in the composition map. Then the "clue values" in the first library of a {9 × 6} array was subsequently utilized to design a further screening in the second library (9 × 6 array, 54 compositions) with a narrower Eu-doping content of 0.02–0.07 mol, which went through the same preparation procedures as above.

Through the above-mentioned two-step combinatorial screening process, two groups of optimized compositions with high luminescence intensity were obtained: $Ca_yY_{3-y}Al_{5-y}Si_yO_{12}$:$Eu_{0.03}$ ($y = 0.5, 1, 1.5$) and $Sr_yY_{3-y}Al_{5-y}Si_yO_{12}$:$Eu_{0.02}$ ($y = 0.1, 0.3, 0.5$). Therefore, larger scale powder phosphors with the optimal compositions were optioned and synthesized by conventional solid-state reaction methods for further heat treatment and characterization.

2.2 Synthesis of powders with optimal compositions

To verify the effectiveness of the screened optimal compositions and to carry out further spectral experiments and characterizations, larger scale powder samples with optimal compositions were prepared by a multi-step solid-state reaction. The raw materials CaO (AR), SrO (AR), Y_2O_3 (4N), Al_2O_3 (AR), SiO_2 (AR), and Eu_2O_3 (4N) were weighed according to the stoichiometric ratio of the optimal compositions $Ca_xY_{3-x}Al_4SiO_{12}$:$Eu_{0.03}$ ($x = 0.5, 1.0, 1.5$) and $Sr_yY_{3-y}Al_{5-y}Si_yO_{12}$:$Eu_{0.02}$ ($y = 0.1, 0.3, 0.5$). The starting powders were thoroughly ground and mixed in an agate mortar with alcohol as a medium. Thereafter, the powder mixture was placed in corundum crucibles and calcined at 900 °C for 4 h in an air atmosphere, ground again, and then calcined at 1400 °C for 5 h in an air atmosphere to obtain powder samples. A part of the obtained powders was further annealed at 600–1300 °C for 1 h in a weak reducing atmosphere (RA, 5% H_2 + 95% Ar) to fabricate phosphor samples Eu-doped with mixed-valence states, because the Eu^{2+} and Eu^{3+} ions can emit light at different wavelengths, to help realize spectral tuning. Moreover, to prove the reversibility of the $Eu^{3+} \leftrightarrow Eu^{2+}$ valence state transition process, the reductively annealed phosphors were divided into several parts and further annealed several times in an air atmosphere as oxidation treatment. Additionally, a pure YAG sample without Eu doping was also prepared with the same heat treatment parameters for comparison.

2.3 Materials characterization

The phase formation and crystal structure of the prepared samples were characterized by a Bruker D8 ADVANCE X-ray diffractometer with Cu Kα radiation. The XRD patterns were recorded in the 10°–90° 2θ range with 5° min^{-1} scanning speed and 0.02° intervals. The photoluminescence (PL) and photoluminescence excitation (PLE) spectra were measured using an F-4600 fluorescence spectrometer from Hitachi with a 150 W xenon light source (the monitoring wavelength ranged from 200 to 900 nm). Temperature-dependent fluorescence spectrum analysis was carried out on a TAP-02 type high-temperature fluorescence controller (Orient KOJI instrument Co., Ltd, temperature range: room temperature–300 °C). The thermoluminescence (TL) data of the samples were recorded using an SL08 thermoluminescence spectrometer with a 3 W mercury lamp (wavelength: 253.7 nm) as the radiation source (Guangzhou Radiation Company, China). The TL spectra were measured from room temperature to 300 °C at a heating rate of 1 °C s^{-1} and the photomultiplier tube voltage was 300 V.

3. Results and discussion

3.1 Combinatorial screening of the composition

Fig. 2(a) illustrates the designed composition map of the initial {9 × 12} array library, containing 108 compositions. Eu ions with 9 increasing contents ($x = 0.001$–0.05 mol) were doped into 12 different matrices as indicated in the first row and first column, respectively. The compositions in rows 1–2 were designed for comparison, only including Eu doping without dual-ion substitution and Eu doping with single Si^{4+} substitution in the YAG matrix. In rows 3–10, considering that the valence state, ligand number, or radius of the substituted divalent ions of Me^{2+} and also Y^{3+} ion, that is Mg^{2+} (0.89 Å, ligand number VIII), Ca^{2+} (1.12 Å, ligand number VIII), Sr^{2+} (1.26 Å, ligand number VIII), Ba^{2+} (1.42 Å, ligand number VIII) and Y^{3+} (1.02 Å, ligand number VIII), were close to Eu ions (1.01 Å for Eu^{3+} and 1.25 Å for Eu^{2+}, ligand number VIII), it was difficult to predict the final occupancy situation of the doped Eu ions, therefore, the corresponding Eu-doping content (x) was designed as an extra component in the matrix. In rows 11–12, two special cases were designed for comparison: one for Mg^{2+} substituting Al^{3+} and one for tri-ion substitution of Sr^{2+} for Y^{3+}, Mg^{2+} for Al^{3+}, and Si^{4+} for Al^{3+} as well.

As vividly depicted in Fig. 2(b), the fluorescence intensity images of the prepared {9 × 12} library were recorded using a CCD camera under 254 nm UV excitation, showing the typical orange–red emission from the 4f–4f transition of Eu^{3+}. Direct observation of the recorded image revealed that the composition region with higher fluorescence intensity was concentrated in the CYASG, SYASG, and BYASG samples with 2–5 mol% Eu^{3+} doping and dual-substituted by Ca^{2+}/Si^{4+}, Sr^{2+}/Si^{4+}, and Ba^{2+}/Si^{4+} ions (located at rows 5–9, columns 6–9, framed by the red line). Since the library was calcined at 1300 °C for 2 h in an air atmosphere, it showed orange–red emission from the 5d → 4f energy level transition of Eu^{3+} ions under 254 nm UV excitation. The luminescence intensity of each composition with a doping concentration lower than 1 mol% was quite weak and could not

(a)

	0.001	0.003	0.005	0.007	0.01	0.02	0.03	0.04	0.05
YAG	$Y_{3-x}Al_5O_{12}$:Eu_x								
YASG	$Y_{3-x}Al_4SiO_{12}$:Eu_x								
MYASG	$Mg_{0.5}Y_{2.5}Al_{4.5}Si_{0.5}O_{12}$:$Eu_x$								
MYASG	$Mg_{1.5}Y_{1.5}Al_{3.5}Si_{1.5}O_{12}$:$Eu_x$								
CYASG	$Ca_{0.5}Y_{2.5}Al_{4.5}Si_{0.5}O_{12}$:$Eu_x$								
CYASG	$Ca_{1.5}Y_{1.5}Al_{3.5}Si_{1.5}O_{12}$:$Eu_x$								
SYASG	$Sr_{0.5}Y_{2.5}Al_{4.5}Si_{0.5}O_{12}$:$Eu_x$								
SYASG	$Sr_{1.5}Y_{1.5}Al_{3.5}Si_{1.5}O_{12}$:$Eu_x$								
BYASG	$Ba_{0.5}Y_{2.5}Al_{4.5}Si_{0.5}O_{12}$:$Eu_x$								
BYASG	$Ba_{1.5}Y_{1.5}Al_{3.5}Si_{1.5}O_{12}$:$Eu_x$								
YMASG	$Y_{3-x}MgAl_3SiO_{12}$:Eu_x								
SYMASG	$SrY_2MgAl_3Si_2O_{12}$:Eu_x								

(b)

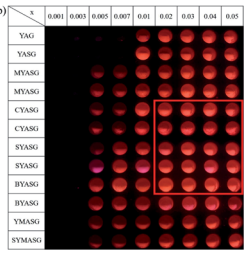

Fig. 2 (a) Designed composition map for the initial screening and (b) fluorescence intensity images of the prepared {9 × 12} library $Me_yY_{3-y}Al_{5-y}Si_yO_{12}$:$Eu_x$ (Me = Mg, Ca, Sr, Ba; $x = 0.001$–0.05, $y = 0.5$, 1.5), recorded under 254 nm UV excitation, herein the y value was changed for the different matrices as marked, and the library was calcined at 1300 °C for 2 h in an air atmosphere.

even be captured by the CCD device at the same time. In addition, the fluorescence intensity of the optimal composition was also slightly higher than that of the YAG:Eu samples without dual-ion substitution (row 1), which could preliminarily indicate that the dual substitution strategy had a positive effect on enhancing the emission intensity of Eu^{3+} ions, owing to the shrinkage of the unit cell and strengthening of the crystal field caused by the dual-ion substitution. Therefore, the compositions within the red frame were selected for the final round of library preparation and for further screening.

Based on the "clue compositions", a {9 × 6} array library with 54 compositions was prepared and subsequently screened with the formula $Me_yY_{3-y}Al_{5-y}Si_yO_{12}:Eu_x$ (Me = Ca, Sr, Ba, x = 0.02–0.07, y = 0.1–1.5). It's worth noting that the over-substitution of Si^{4+}($y > 1$) may induce a second phase of silicate in YAG hosts. Besides, it was also found in the previous research that ions with a larger radius, such as Sr^{2+} and Ba^{2+}, also contribute to the generation of the second phase after entering the dodecahedron sites of the YAG host through substitution. Thus, for the further screening of the library, the substitution amounts of Si^{4+}, Sr^{2+}, and Ba^{2+} ions were reduced to 10, 30, and 50 mol% to obtain a high purity of the garnet phase. The designed composition map is shown in Fig. 3(a). The concentration of Eu^{3+}-ion doping was extended to 2–7 mol% from top to bottom with an interval of 1 mol%, since concentration quenching of the activator ion Eu^{3+} was not observed during the preliminary screening process, as indicated in Fig. 2(b).

Fig. 3(b) shows the fluorescence images of the {9 × 6} library under 254 nm excitation recorded by a CCD camera with auto-sensitivity (ISO = 250, 50). The upper-left region with high fluorescence intensity could barely be distinguished by direct observation. In order to fully expose the compositions with higher fluorescence intensity and obtain more accurate comparison results, the camera ISO was also manually adjusted to a lower value of 50 when recording. After that, two groups of compositions with higher luminescence intensity were selected, as indicated by the two red frames in Fig. 3(b). Also, the optimal compositions could be initially identified as $Ca_yY_{3-y}Al_{5-y}Si_yO_{12}:Eu_{0.03}$ in row 2 (y = 0.5, 1, 1.5; simplified as $Ca_{0.5}$, Ca_1, $Ca_{1.5}$) and $Sr_yY_{3-y}Al_{5-y}Si_yO_{12}:Eu_{0.02}$ in row 1 (y = 0.1, 0.3, 0.5; simplified as $Sr_{0.1}$, $Sr_{0.3}$, $Sr_{0.5}$). To verify if the emission intensity change of the powders was consistent with the combinatorial screening results, powder samples with the two groups of optimal compositions were further prepared by a solid-state reaction method and then characterized.

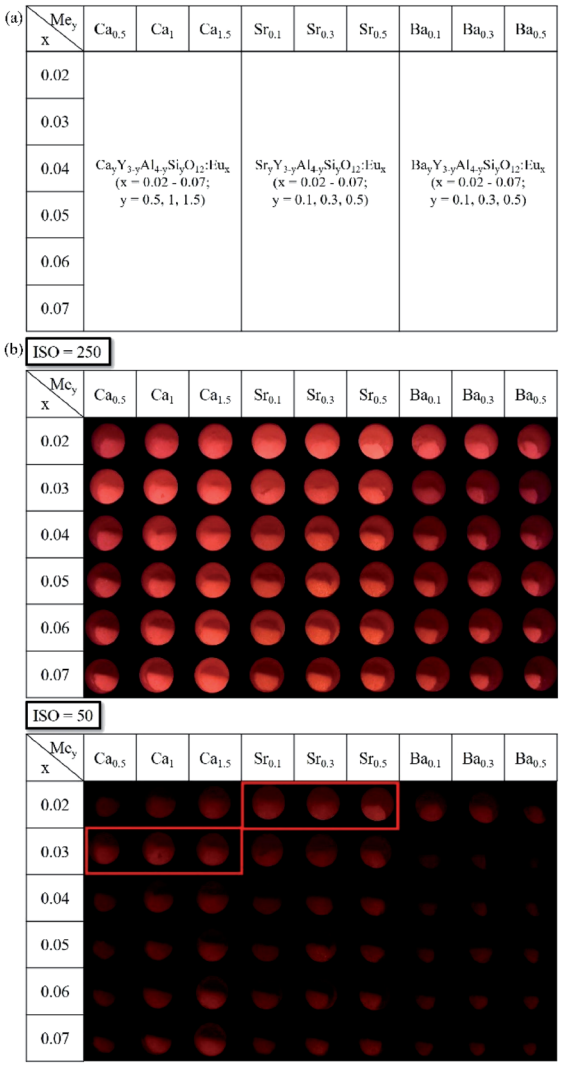

Fig. 3 (a) Designed composition map for further screening and (b) fluorescence images of the $Me_yY_{3-y}Al_{5-y}Si_yO_{12}:Eu_x$ (Me = Ca, Sr, Ba; x = 0.02–0.07, y = 0.1–1.5) library under 254 nm excitation, the library was calcined at 1300 °C for 2 h in an air atmosphere.

3.2 Luminescence property of the powders with the optimal compositions

Based on the combinatorial screening results mentioned above, optimal composition phosphors of $Ca_yY_{3-y}Al_{5-y}Si_yO_{12}:Eu_{0.03}$ (y = 0.5, 1, 1.5) and $Sr_yY_{3-y}Al_{5-y}Si_yO_{12}:Eu_{0.02}$ (y = 0.1, 0.3, 0.5) were prepared by a solid-state reaction at 1400 °C for 5 h in an air atmosphere and their emission spectra were characterized as indicated in Fig. 4. At this stage, the orange–red emissions in

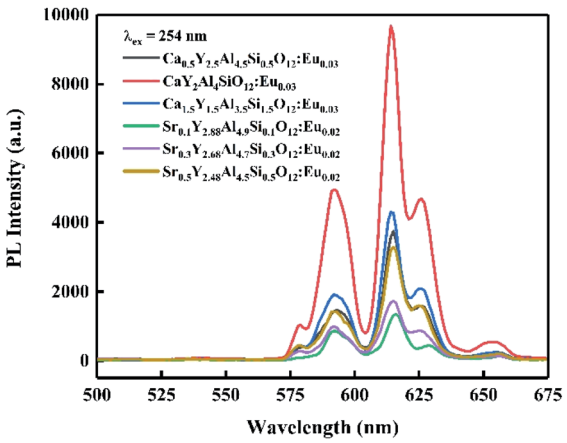

Fig. 4 Emission spectra of $Ca_yY_{3-y}Al_{5-y}Si_yO_{12}:Eu_{0.03}$ (y = 0.5, 1, 1.5) and $Sr_yY_{3-y}Al_{5-y}Si_yO_{12}:Eu_{0.02}$ (y = 0.1, 0.3, 0.5) phosphors (λ_{ex} = 254 nm), calcined at 1400 °C for 5 h in an air atmosphere.

the spectra were mainly from the $^5D_0 \rightarrow {}^7F_J$ ($J = 1, 2$) transition of trivalent Eu^{3+} ions. Among these, the Ca-containing sample of $CaY_2Al_4SiO_{12}:Eu_{0.03}$ ($y = 1$) showed a significantly higher PL intensity than the other samples, and the PL intensities of the Ca^{2+}/Si^{4+} dual-substituted samples were all higher than those of the Sr^{2+}/Si^{4+} dual-substituted samples. The relative PL intensity ranking of the powder samples was: $Ca_1 > Ca_{1.5} > Ca_{0.5} > Sr_{0.5} > Sr_{0.3} > Sr_{0.1}$. Furthermore, from the structural analysis, as shown in Fig. 5, the XRD spectra for both the high-Ca-substituted $CaY_2Al_4SiO_{12}:Eu_{0.03}$ and low-Ca-substituted $Ca_{0.5}Y_{2.5}Al_{4.5}Si_{0.5}O_{12}:Eu_{0.03}$ samples matched well with the $Y_3Al_5O_{12}$ standard pattern (PDF #73-1370), indicating that the multi-components design with Eu doping and dual-ion substitution was within a reasonable solid-solution range of the $Y_3Al_5O_{12}$ matrix. Relatively, the $CaY_2Al_4SiO_{12}:Eu_{0.03}$ sample had a higher phase purity compared to the low-Ca-substituted $Ca_{0.5}Y_{2.5}Al_{4.5}Si_{0.5}O_{12}:Eu_{0.03}$ sample, which showed slightly obvious and weak diffraction peaks of the impurity phase $Ca_4Y_6O(SiO_4)_6$ (PDF #27-0093). Moreover, the synthesis temperature and soaking time of $Ca_4Y_6O(SiO_4)_6$ were very close to that of CYASG:Eu, hence it was quite difficult to avoid the impurity. Fortunately, the content of the impurities was very low, and there was no negative effect on the luminescence properties. Since the compositions of the two samples were both designed as extra Eu-ions doping in the matrix, which must inevitably lead to a little excess of Ca, Y and other elements owing to the random occupation of the doped Eu ions at the substitution sites, the formation of a small amount of impurity phase was expected. Thus, the composition of $CaY_2Al_4SiO_{12}:Eu_{0.03}$ (abbreviated to CYASG:Eu) was chosen for further annealing treatment in a weak reductive atmosphere (RA-annealing) to realize the transition of Eu^{3+} to Eu^{2+} and also for the spectral tuning.

3.2.1 Spectral tuning of CYASG:Eu powders *via* RA-annealing. Fig. 6 presents the emission spectra of the optimal CYASG:Eu samples without and with annealing treatment at 1100 °C for 4 h in RA, excited by 254 nm UV light. Compared with the sample without RA-annealing (black spectrum), the annealed sample exhibited a wide and very high PL band (red spectrum) from 380 to 520 nm, which should be assigned to the

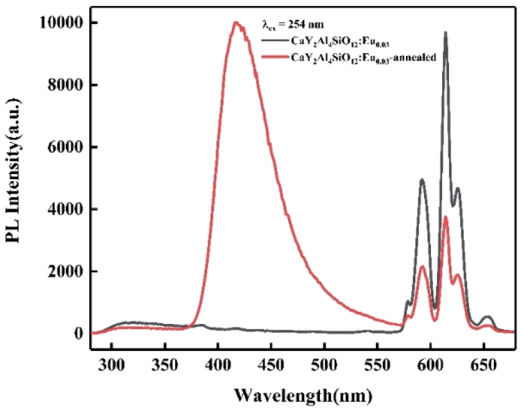

Fig. 6 Emission spectra of CYASG:Eu with and without RA-annealing at 1100 °C for 4 h, $\lambda_{ex} = 254$ nm.

$4f^65d^1 \rightarrow 4f^7$ transition of Eu^{2+}. It is speculated that part of the originally doped Eu^{3+} ions had been reduced to the stable lower valence states of Eu^{2+}. Furthermore, the annealing treatment in RA did not cause obvious effects on the crystal phase composition of the two samples, besides the weak diffraction peaks of the impurity phases, as seen in Fig. 5 again.

3.2.2 Annealing time-dependent spectral property of CYASG:Eu. The annealing duration at high temperature has a significant effect on the emission character. Fig. 7 shows the emission spectra of the CYASG:Eu samples under 254 nm UV excitation after RA-annealing at 1100 °C for 1 h and 5 h, with the YAG matrix sample without doping used for reference. In addition to the orange–red emission (4f–4f transition of Eu^{3+}) around 600 nm, a strong blue emission peak from Eu^{2+} (5d–4f transition) could be observed in the range from 380 to 520 nm with a peak wavelength of 418 nm. The spectrum of the pure YAG matrix sample (red line) ruled out the possibility of the blue emission from the matrix. Also, for the samples with longer treatment time in the reducing atmosphere, more Eu^{3+} ions are reduced into Eu^{2+}. Extending the treatment duration properly would increase the crystallinity of phosphor samples, thereby enhancing the PL intensity of the sample that is RA-annealed for longer than 5 h.

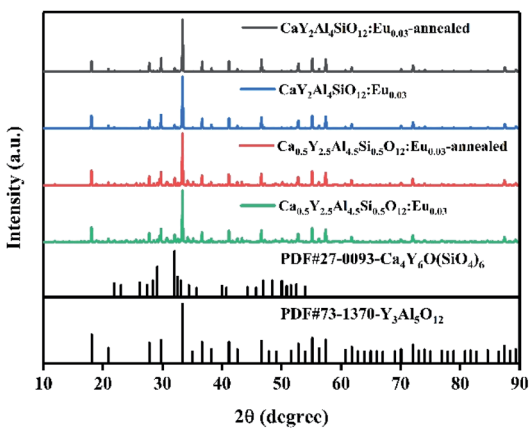

Fig. 5 XRD spectra of $CaY_2Al_4SiO_{12}:Eu_{0.03}$ and $Ca_{0.5}Y_{2.5}Al_{4.5}Si_{0.5}O_{12}:Eu_{0.03}$ samples with and without RA-annealing at 1100 °C for 4 h.

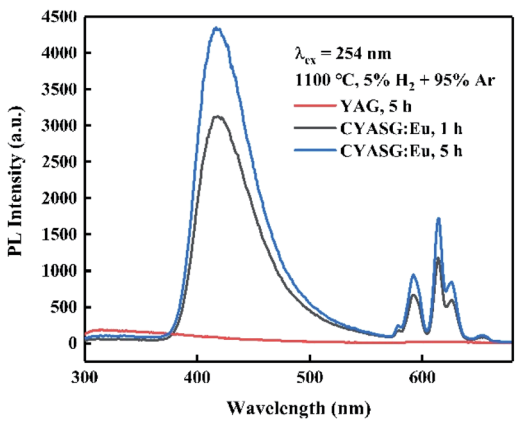

Fig. 7 Emission spectra of CYASG:Eu samples after RA-annealing at 1100 °C for 1 h and 5 h, $\lambda_{ex} = 254$ nm.

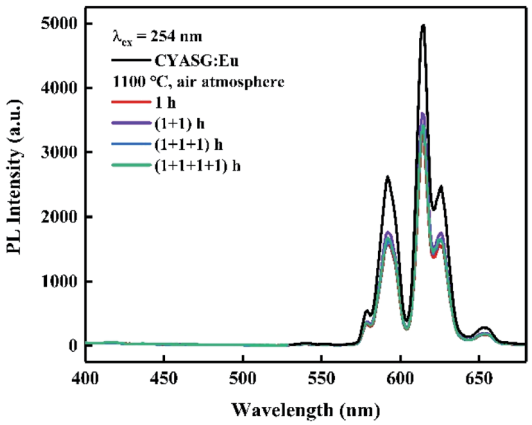

Fig. 8 Emission spectra of the RA-annealed CYASG:Eu samples after four times of re-treatment at 1100 °C for 1 h in air, λ_{ex} = 254 nm.

To verify the reversibility of the $Eu^{3+} \leftrightarrow Eu^{2+}$ transition, the samples RA-annealed at 1100 °C for 4 h were re-treated at 1100 °C for 1 h in an air atmosphere for several rounds. Fig. 8 shows the emission spectra variations of the RA-annealed CYASG:Eu samples under 254 nm excitation after 4 times of re-treatment at 1100 °C for 1 h in air. The emission in the region 380–520 nm from Eu^{2+} ions completely disappeared, while the PL intensity of the orange–red emission from Eu^{3+} gradually decreased with the time increasing for re-treatment in air. The emission intensity degradation could be attributed to the multiple re-treatments at 1100 °C in air that might induce defect formation in the lattice or on the surface of the powders.

3.2.3 Annealing temperature-dependent spectral property of CYASG:Eu. Besides the annealing duration, the annealing temperature also has a remarkable influence on the crystallization and resultant spectral properties of phosphors. The XRD patterns of the CYASG:Eu samples RA-annealed in a wide temperature range from 800–1300 °C for 1 h are indicated in Fig. 9(a), with the unannealed sample shown as a comparison. All the RA-annealed samples showed no obvious difference in XRD patterns with the YAG standard pattern (PDF #73-1370). The weak impurity phase peaks could be matched with $Ca_4Y_6O(SiO_4)_6$ (PDF #27-0093), due to the relative "excess" of Ca and Y ions in the matrix caused by the extra doping of Eu ions of 0.03 mol. With the increase in annealing temperature, the diffraction peaks in the 2θ range from 33° to 34° were shifted slightly to the lower angle side as shown in Fig. 9(b). Also, more Eu^{3+} was reduced to Eu^{2+} in the matrix lattice. As a consequence, the substitution of smaller Eu^{3+} (r = 1.07 Å, CN = 8) by larger Eu^{2+} (r = 1.25 Å, CN = 8) will lead to cell expansion, resulting in a unit cell volume as well as lattice constant increase when the concentration of Eu^{2+} is increased, as demonstrated in Table 1, where R800, R900, R1000, R1200, and R1300 represent CYASG:Eu samples annealed at 800 °C, 900 °C, 1000 °C, 1200 °C, and 1300 °C for 1 h in a reductive atmosphere, respectively.

It must be noted that when the RA-annealing temperature was reduced to 600 °C for 1 h (shortened as R600), there was no blue emission from Eu^{2+} ions compared with the emission

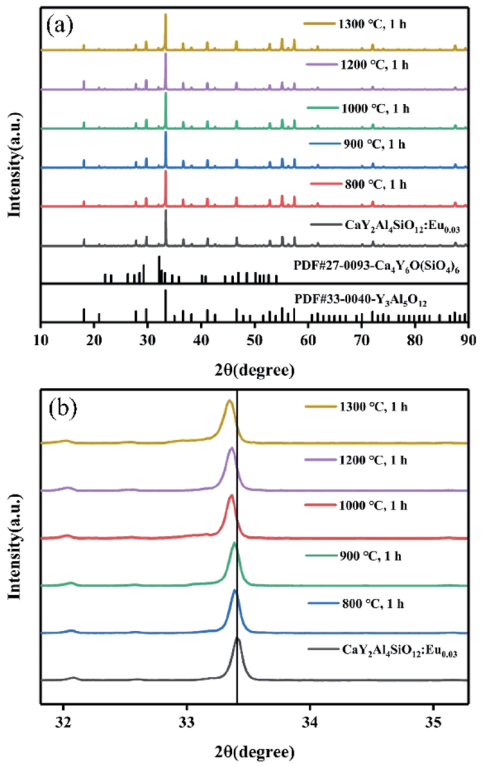

Fig. 9 XRD patterns of CYASG:Eu samples RA-annealed at 800 °C, 900 °C, 1000 °C, 1200 °C, and 1300 °C for 1 h, (a) $2\theta = 10°–90°$ and (b) $2\theta = 32°–35°$.

spectrum of R800 as illustrated in Fig. 10. It could be inferred that the valence transition from Eu^{3+} to Eu^{2+} starts in the temperature range of 600–800 °C. Moreover, the excitation spectra PLE (λ_{em} = 420 nm and 615 nm) of R800 are illustrated in Fig. 11. Monitoring at 615 nm, the PLE spectrum showed a broad band centered at 230 nm, which belonged to the Eu^{3+}–O^{2-} charge-transfer band. While monitoring at 420 nm, the measured broad "hump" excitation band ranging from 200–400 nm was attributed to the $4f^7$–$4f^65d^1$ energy level transition of divalent Eu^{2+} ions. This further confirmed the coexistence of two luminescence centers Eu^{2+}/Eu^{3+} in the R800 sample.

In addition, with a higher RA-annealing temperature employed, the orange–red emission from Eu^{3+} ion weakened, and the emission peak from Eu^{2+} ion (400–500 nm) was significantly increased and gradually dominated, as shown in Fig. 12(a). Surprisingly, the integrated PL intensity of the R1300

Table 1 Lattice parameters of CYASG:Eu RA-annealed at different temperatures

Sample	Lattice constant (Å)	Cell volume (Å)	R (Å)
CYASG:Eu	11.9906	1723.93	7.1
R800	11.9935	1725.18	6.4
R900	11.9945	1725.63	6.8
R1000	11.9982	1727.24	7.5
R1200	11.9985	1727.34	7.7
R1300	12.0005	1728.23	8.7

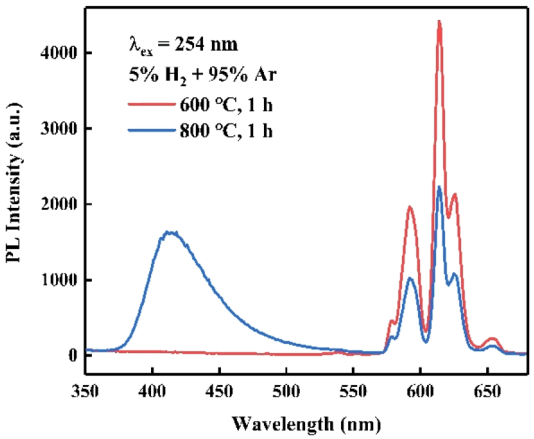

Fig. 10 Emission spectra of R600 and R800 samples, λ_{ex} = 254 nm.

sample was 4.65 times higher than that of sample annealed at 600 °C, as seen in Fig. 12(b). This further indicated that more Eu^{3+} ions are reduced into Eu^{2+} with the assistance of RA-annealing treatment and the high emission efficiency of Eu^{2+} ions in CYASG matrix.

3.2.4 Thermal stability and trap effect of CYASG:Eu. The temperature-dependent PL spectra of R800 are shown in Fig. 13(a). With the temperature increasing, the integrated PL intensity of the sample was enhanced abnormally at the beginning, and the highest PL intensity was obtained at 75 °C (blue spectrum). Then, the PL intensity dropped to the level above that measured at room temperature after passing the temperature range of 100–125 °C. Finally, the emission intensity decreased greatly up to ~85% and ~63% of its initial value at 175 °C and 250 °C, respectively. The integrated PL intensity–temperature curve was calculated and is illustrated in Fig. 13(b), based on the measured results from Fig. 13(a) (integration range: 360–535 nm and 583–680 nm). It is obvious that in the temperature range of 50–100 °C, the sample gave an intensity 105–110% that of the fluorescence emission measured at room

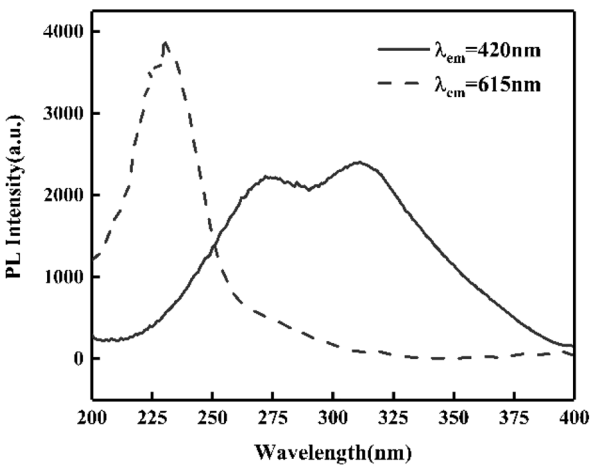

Fig. 11 Excitation spectra of the R800 sample, λ_{em} = 420 nm and 615 nm.

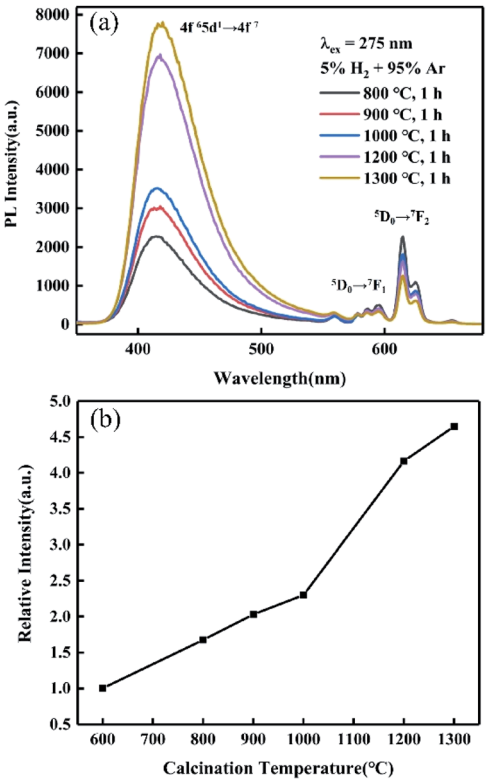

Fig. 12 (a) Emission spectra and (b) integrated emission intensity variation curve of CYASG:Eu samples RA-annealed in the range 800–1300 °C for 1 h, λ_{ex} = 275 nm.

temperature, and this could also be maintain at about 63% that of the room temperature emission at a high of 250 °C. This shows that the R800 sample had excellent thermal quenching resistance.

In order to find out the possible reasons for the abnormally enhanced emission, the thermoluminescence (TL) spectra, as illustrated in Fig. 14, were recorded to study the migration of excited carriers under heating as well as the trap depth, because TL measurement is one of the most effective ways to detect the concentration and distribution of defects or traps.[29] The corresponding trap depth of the R800 sample was 0.701 eV, which could be roughly estimated by the classic formula $E = 500/T_m$, where E (eV) is the trap depth and T_m (K) is the temperature of the TL peak. The TL peak temperature of the R800 sample was about 75 °C which may correlate with its abnormally enhanced emission at 50–100 °C (Fig. 13(b)). The abnormal increase of emission between 50–100 °C was likely caused by the release of the electrons or charge carriers captured in the traps when the phosphors were excited by incident light at high temperature; that is, the electrons or charge carriers captured by traps can be gradually released to continuously compensate for the luminescence intensity loss due to normal temperature quenching under the more intensive disturbance of thermal energy. Furthermore, this abnormal temperature region of 50–100 °C is fantastically consistent with the above TL band centered at 77.28 °C, meaning that the abnormal increase in PL intensity is directly linked to the properties of the traps and the behaviors of

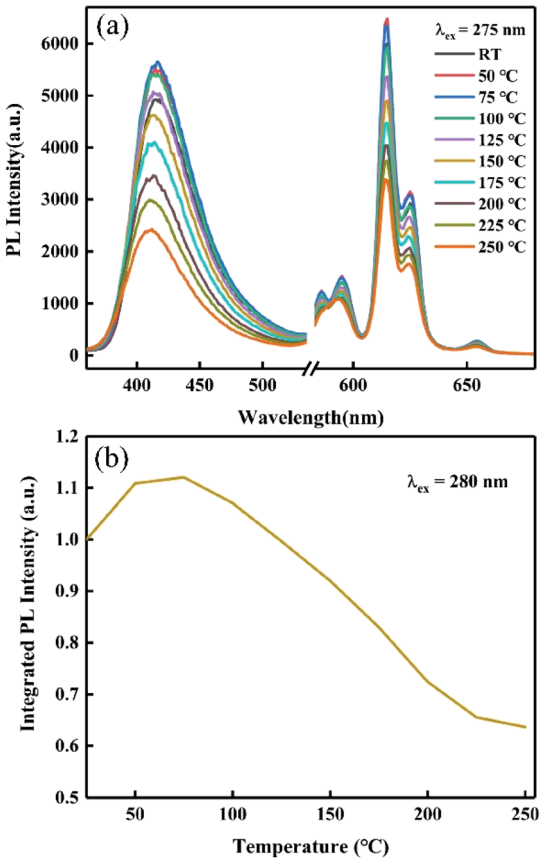

Fig. 13 (a) Temperature-dependent PL spectra and (b) integrated intensity–temperature curve of R800, λ_{ex} = 275 nm.

the electrons or carriers captured by the traps. The further decrease of the luminescence intensity above 125 °C is likely from the normal non-radiative transition occurring in the higher temperature heating process, and because of the much higher thermal energy over 125 °C, the carriers or electrons stably captured in the traps are fewer and thus it is more difficult to continuously compensate for the loss of emission intensity. As for the traps or defects origination in the R800 sample, they likely resulted from oxygen vacancies and other lattice defects owing to the annealing in the reductive atmosphere, in line with some previous research on oxygen vacancy defects formation *via* reducing- and vacuum-atmosphere heat treatment.[30,31]

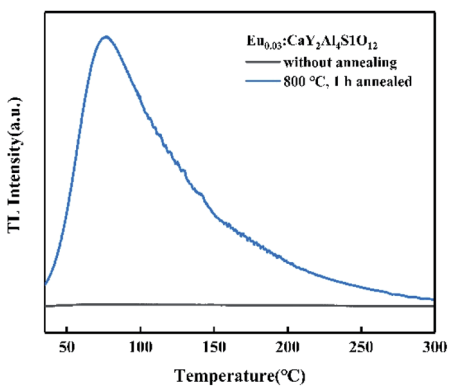

Fig. 14 TL spectrum of the R800 sample.

4. Conclusions

By a dual-ion substitution strategy, fluorescent material libraries of $Me_yY_{3-y}Al_{5-y}Si_yO_{12}$:$Eu_x$ were prepared by a combinatorial method in parallel microreactors and the optimal compositions were obtained through a rapid luminescence screening under ultraviolet irradiation of 254 nm. The reliability of the combinatorial screening results were verified by comparing with the corresponding powder samples prepared in parallel solid-state synthesis, confirming an optimal composition of $Ca_yY_{3-y}Al_{5-y}Si_yO_{12}$:$Eu_{0.03}$ (CYASG:Eu) with the highest luminescence intensity.

Fluorescence characterization of the optimal CYASG:Eu samples annealed in a weak reducing atmosphere (RA) demonstrated the coexistence of divalent/trivalent Eu ions, and reversibility of the $Eu^{3+} \leftrightarrow Eu^{2+}$ valence transition process was possible by controlling the temperature, duration, and atmosphere of annealing. As a result, the dominant emissions can be effectively tuned from the orange–red lighting of Eu^{3+} (f–f transition) to the blue lighting of Eu^{2+} (5d–4f transition).

With the generation of Eu^{2+}, the integrated intensity of the PL spectrum obviously increased. The temperature-dependent photoluminescence spectra of the RA-annealed CYASG:Eu phosphors showed excellent thermal quenching resistance, at ~110% of the room temperature PL intensity under 75 °C measurement condition and ~63% at 250 °C. The TL spectrum proved the existence of trap energy levels in the phosphors that may compensate for the emission loss to some extent at the corresponding temperatures and can also explain the abnormal increase in the PL intensity in the 50–100 °C region.

This research work shows the high efficiency and reliability of the combinatorial preparation and screening of dual-ion substituted YAG-based phosphors. By combination of the double substitution of cation ions and RA-annealing, we provide a new approach to create the coexistence of activators with mixed-valence states in the YAG system. The prepared CYASG:Eu phosphors possessed a highly tunable spectra property and excellent thermal stability and they showed application prospects in the field of plant light supplement as luminescent materials for energy-saving light sources.

Author contributions

Zhehan Zheng contributed to writing – original draft and experimental operation; Mingxue Deng contributed to manuscript preparation with constructive discussions. Caiyan Wang performed the guidance of instruments. Xiang Zhang helped to perform the experiment; Qian Liu contributed significantly to writing – review & editing; Xiaoke Xu and Le Gao helped to set up experimental apparatus.

Conflicts of interest

There are no conflicts to declare.

Acknowledgements

Many thanks for the financial supports from the National Key Research and Development Program of China (grant no. 2016YFB0700204 and 2018YFB0704103) and the Foundation of Shanghai Science and Technology Committee (grant no. 18511110400).

References

1 Y. Wang, G. Zhu, S. Xin, Q. Wang, Y. Li, Q. Wu, C. Wang, X. Wang, X. Ding and W. Geng, *J. Rare Earths*, 2015, **33**, 1–12.
2 H. S. Jang, W. B. Im, C. L. Dong, D. Y. Jeon and S. K. Shi, *J. Lumin.*, 2007, **126**, 371–377.
3 L. Wang, X. Zhang, Z. Hao, Y. Luo and J. Zhang, *Opt. Express*, 2010, **18**, 25177–25182.
4 T. Gao, J. Tian, Y. Liu, R. Liu and W. Zhuang, *Dalton Trans.*, 2021, **50**, 3769–3781.
5 D. Sun, L. Zhang, Z. Hao, H. Wu, H. Wu, Y. Luo, L. Yang, X. Zhang, F. Liu and J. Zhang, *Dalton Trans.*, 2020, **49**, 17779–17785.
6 R. J. Xie, N. Hirosaki, N. Kimura, K. Sakuma and M. Mitomo, *Appl. Phys. Lett.*, 2007, **90**, 191101.
7 W. Wang, J. Tang, T. H. Sheng, W. Jing and B. P. Sullivan, *Chem. Phys. Lett.*, 2008, **457**, 103–105.
8 H. Yang and Y. S. Kim, *J. Lumin.*, 2008, **128**, 1570–1576.
9 Q. Du, S. Feng, H. Qin, H. Hua, H. Ding, L. Jia, Z. Zhang, J. Jiang and H. Jiang, *J. Mater. Chem. C*, 2018, **6**, 12200–12205.
10 X. Ding, W. Geng, Q. Wang and Y. Wang, *RSC Adv.*, 2015, **5**, 98709–98716.
11 Y. Shi, Z. Ge, M. Mikami, Y. Shimomura and Y. Wang, *Dalton Trans.*, 2014, **44**(4), 1775–1781.
12 Y. Xiao, W. Xiao, L. Zhang, Z. Hao, G. H. Pan, Y. Yang, Z. Xia and J. Zhang, *J. Mater. Chem. C*, 2018, **6**, 10–1039.
13 C. C. Chiang, M. S. Tsai and M. H. Hon, *J. Electrochem. Soc.*, 2007, **154**, J326.
14 J.-G. Li and Y. Sakka, *Sci. Technol. Adv. Mater.*, 2015, **16**, 14902–14919.
15 M. Shang, J. Fan, H. Lian, Y. Zhang, D. Geng and J. Lin, *Inorg. Chem.*, 2014, **53**, 7748–7755.
16 Y. Zhou, J. Lin, Y. Min, S. Wang and H. Zhang, *Mater. Lett.*, 2002, **56**, 628–636.
17 M. Shang, C. Li and J. Lin, *Chem. Soc. Rev.*, 2014, **43**, 1372–1386.
18 G. Y. Lee, J. Y. Han, W. B. Im, S. H. Cheong and D. Y. Jeon, *Inorg. Chem.*, 2012, **51**, 10688–10694.
19 V. Tsiumra, A. Krasnikov, S. Zazubovich, Y. Zhydachevskyy and A. Suchocki, *J. Lumin.*, 2019, **213**, 278–289.
20 C. Yang, G. Song, J. Miao and T. Fan, *Dalton Trans.*, 2021, **50**, 3769–3781.
21 I. E. Kolesnikov, D. V. Mamonova, M. A. Kurochkin, E. Y. Kolesnikov and E. Lhderanta, *Opt. Mater.*, 2021, **112**, 110797.
22 M. Sugiyama, T. Yanagida, Y. Fujimoto, Y. Yokota, A. Ito, M. Nikl, T. Goto and A. Yoshikawa, *Opt. Mater.*, 2012, **35**, 222–226.
23 Y. Chen, D. Feng, S. Xu, S. Zeng and X. Wei, *Mater. Lett.*, 2016, **164**, 180–182.
24 G. A. Petrosyan, R. H. Asatryan, L. K. Hovhannesyan, V. M. Derdzyan and P. S. Feofilov, *Mater. Chem. Phys.*, 2017, **185**, 39–43.
25 Q. Q. Zhu, W. W. Hu, L. C. Ju, L. Y. Hao, X. Xu and S. Agathopoulos, *J. Am. Ceram. Soc.*, 2013, **96**, 701–703.
26 Z. Ming, J. Qiao, M. S. Molokeev, J. Zhao and Z. Xia, *Inorg. Chem.*, 2020, **59**, 1405–1413.
27 L. Havlák, J. Bárta, M. Buryi, V. Jarý, E. Mihóková, V. Laguta, P. Boháček and M. Nikl, *J. Phys. Chem. C*, 2016, **120**, 21751–21761.
28 Z. Pan, J. Chen, H. Wu and W. Li, *Opt. Mater.*, 2017, **72**, 257–264.
29 K. Eeckhout, A. Bos, D. Poelman and P. F. Smet, *Phys. Rev. B*, 2013, **20**, 196.
30 J. Trojan-Piegza and E. Zych, *J. Phys. Chem. C*, 2014, **114**, 4215–4220.
31 J. Trojan-Piegza, J. Niittykoski, J. Hoelsae and E. Zych, *Chem. Mater.*, 2008, **20**, 2252–2261.